Influence of Calcium Treatment and Electromagnetic Stirring on Ridging in Dual-Stabilized Ferritic Stainless Steels

Suresh Kodukula*, Marko Petäjäjärvi, Jari Savolainen, Timo Fabritius, David Porter

Suresh Kodukula
Tornio Research Center, Outokumpu Stainless Oy,
Terästie 1, 95490, Tornio, Finland
E-mail: suresh.kodukula@outokumpu.com

Marko Petajäjärvi, Jarvi Savolainen
Steel Melting Shop Development, Outokumpu Stainless Oy,
Terästie 1, 95490, Tornio, Finland

Prof. Timo Fabritius
Department of Process Metallurgy, Faculty of Technology, University of Oulu
90014 Oulu, Finland

Emeritus Prof. David Porter
Centre for Advanced Steels Research, Faculty of Technology, University of Oulu
90014 Oulu, Finland

Keywords: Calcium Treatment, Ridging, Electromagnetic Stirring, Titanium and Niobium Stabilization

Titanium and niobium are added to ferritic stainless steels to enhance their surface and mechanical properties. The use of titanium to obtain ferritic stainless steel sheets that are resistant to ridging due to the formation of equiaxed rather than columnar grains during solidification is well established. However, the use of titanium results in the clogging the submerged entry nozzle during casting causing surface defects in cold rolled products and overall production losses. To overcome the clogging problem, calcium treatment is carried out in the ladle furnace to transform inclusions into the liquid state. However, this delays the formation of the TiN inclusions which act as nuclei for

the equiaxed grains, thereby increasing the fraction of columnar grains in the slabs and the susceptibility to ridging in the final cold-rolled and annealed product. In this study, the effect of calcium treatment and electromagnetic stirring on the equiaxed grain ratio and ridging have been studied with industrially produced material. The beneficial effect of EMS on grain structure and ridging is largely lost at high calcium contents, but it can be retained provided the level of calcium can be maintained at a sufficiently low, optimum level.

1. Introduction

Titanium and niobium are added to ferritic stainless steels (FSS) to react with carbon and nitrogen in order to enhance their mechanical and corrosion properties. Such dual-stabilized ferritic stainless steels (FSS) have major benefits compared to grades only stabilized with titanium such as improved surface quality, formability and weldability. Compared to single-stabilized grades, dual-stabilized grades also have higher strength at elevated temperatures, i.e. better resistance against creep and thermal fatigue, as well as better oxidation and corrosion resistance at high temperatures. Most of these benefits occur because of an excess of Nb that remains in solution after the stabilization precipitation reactions have occurred. Due to these properties and their overall cost-effectiveness, dual-stabilized FSS are widely used in e.g. culinary, automobile and calorifier applications.

FSS are often prone to the appearance of a surface defect, known as ridging, which may appear as corrugations along the rolling direction on the surface of the sheet following deep drawing. Products with ridging need additional polishing which increases the production costs. Ridging results from columnar solidification during continuous casting.[1,2] It has been demonstrated that an increase in the ratio of equiaxed to columnar grains after casting, i.e. the equiaxed grain ratio (EGR), leads to significant improvements in ridging resistance.[3–6] When present in sufficient

quantities, as is the case in stabilized FSS, TiN forms above the liquidus temperature of steel, thereby acting as nuclei for equiaxed grains during solidification and increasing EGR.[7,8] Any nitrogen not precipitated from the liquid together with the carbon in the steel are precipitated as Nb(CN) during slab cooling after solidification. Any Ti not precipitated from the liquid will be precipitated in the solid phase as (TiNb)C.[9,10] Dual, Ti +Nb, stabilized FSS steels behave similarly to single Ti-stabilized steels since NbC form after solidification. In addition to TiN, the main types of inclusions found in the dual-stabilized and Ti-stabilized FSS are Al_2O_3 and Al_2O_3-TiO_x-TiN.[9]

Aluminum is added as a deoxidizer before the addition of Ti and Nb to improve the yield of titanium by reducing the formation of titanium oxides.[10–12] In continuous casting, the clogging of the submerged entry nozzle (SEN) in the mold can be problematic leading to reductions in productivity. Thomas et al.,[13,14] classified the origin of the materials causing clogging into four types: 1) deoxidation products, 2) solidified steel, 3) complex oxides and 4) reaction products. The alumina inclusions that result from deoxidation with aluminum are the main cause of clogging in aluminum-killed steels. In addition to causing clogging, deoxidation products can cause surface defects, such as skin laminations or line defects, on the final strip product.[15–17] In addition to alumina inclusions, spinel (Al_2O_3-MgO) inclusions can be generated due to soluble Mg supplied from the MgO-based refractory.[18,19] Clogging problems can be prevented by transforming the solid alumina and spinel into liquid inclusions that do not attach themselves to the SEN. An efficient way of achieving this is to use a calcium treatment.[18,20–25] Jingyu et al [26–28] have shown that a small amount of Ca in Al-killed Ti-bearing 11Cr stainless steel effectively modifies Al_2O_3-TiO_x inclusions into liquid oxide inclusions and reduces the stability of spinel by modifying the solid alumina into liquid calcium aluminate.

While calcium treatment prevents SEN clogging, it has an adverse effect on EGR. The reason for this is that without the presence of solid alumina particles in the melt the nucleation of TiN is difficult. Without TiN, the nucleation of equiaxed grains is hindered and EGR is reduced causing an increase in the incidence of ridging. EGR can be improved using electromagnetic stirring (EMS) of the melt in the mold. The present study was undertaken to evaluate the combined effects of EMS and calcium treatment on the ridging properties of the final cold rolled FSS sheet.

2. Materials and Methods

2.1 Experimental

Titanium and niobium stabilized ferritic stainless steels were produced using an electric arc furnace (EAF) followed by an argon oxygen decarburization (AOD) converter. In the EAF process, stainless scrap and alloys were melted and ferrochrome (FeCr) added to make the total steel melt of approximately 80 tons. The liquid steel was then decarburized, deoxidized and desulfurized in the AOD converter. The alloying and cooling scrap additions increase the weight in the AOD converter to 95 tons. After the AOD processing and slag removal, the liquid steel was tapped into a doloma-lined casting ladle after removing the slag. During ladle furnace refining process, aluminum is added first to achieved de-oxidation. Later the titanium and niobium are added accordingly after calcium treatment with wire. After achieving the target final composition and temperature, the steel melt is transferred to continuous casting platform for casting. Electromagnetic stirrer (EMS) is located 4m below from the meniscus of 900 mm long mold. Trials were carried out on an industrial scale to investigate the effect of calcium treatment and electro-magnetic stirring on the macro-texture after continuous casting and the ridging properties of the final product ensuring that the samples were collected from corresponding locations in the casting sequence.

2.2 Sample collection

Lollipop samples from the liquid steel were collected from every step throughout the EAF, AOD and LF processing and quenched immediately into water. During LF refining, lollipop samples were collected 7-8 min after every process step such as after the addition of Al, end calcium treatment, and after adding the Ti wire. The final LF sample was collected at the end of LF refining before sending ladle to continuous casting. For each heat, slab samples for macrostructure studies were cut between the 2nd and 3rd slabs, where the casting conditions are stable.

All the slabs were re-heated in a walking beam furnace to 1150^{o}C for 150 min and later hot rolled. Samples A-C and E were hot rolled to a thickness of 6 mm and after hot rolling, the coils were annealed, pickled and cold rolled in 24-high Sendzimir mill to the final thickness. After cold rolling, the coils were annealed and pickled, and skin passed in 2-high skin pass mill. The cold reduction in the skin pass mill was between 0.5-1%. Samples A-C and E were hot rolled to a thickness of 6 mm and cold rolled twice to achieve the final thickness, whereas sample D was reduced to 3.5 mm during hot rolling and then cold rolled once to the final thickness of 1.17 mm. All the hot and cold rolling thicknesses and reductions are tabulated below in **Table 1**. Specimens with dimensions 100 mm in transverse direction and 300 mm in rolling direction were cut from each of the coils and strained 15% in tension as explained in section 2.3 to measure the severity of the ridging.

2.3 Methodology

The acid soluble Al, Ca and Mg contents of the steel were determined using inductively coupled plasma optical emission spectrometry (Thermo iSparks 8860) which has a $\pm$ 5 % relative standard deviation. The chemical compositions of the steel specimens are shown in Table 2. Full cross-section, 50 mm thick slab samples were cut with a torch cutting machine at the caster. The slabs

were 1000 - 1650 mm wide and 170 mm thick. 200 mm wide pieces of these were cut across the whole slab thickness to give samples perpendicular to the casting direction. These were ground and polished with 10 μm and 6 μm grit before etching. The polished surface was etched in aqua regia, i.e. a mixture of nitric acid (HNO_3) and hydrochloric acid (HCl), to reveal the macrostructure. The equiaxed grain ratio (EGR) was calculated as the ratio of the total thickness of the equiaxed zone to the slab thickness.[6]

Specimens for ridging tests were cut from the final sheet products at positions corresponding to the locations of the slab samples. Their dimensions were 300 mm in the rolling direction and 100 mm across the sheet width, and they were elongated 15 % in a tensile testing machine using special grips. The unfiltered 2D raw surface profile after the ridging tests was measured using a non-skidded bench-top 2D stylus profilometer Zeiss Surfcom 2000 SD3 with stylus tip radius of 2μm. This raw profile is filtered to calculate the ridging index (RI) a unique index taking into account the height of the profile and the spacing between the ridges.[29] Specimens of 30 mm x 30 mm were also cut from the final sheet for micro-texture measurements using electron backscatter diffraction (EBSD) in a scanning electron microscope (SEM, LEO 1450VP) at 20 kV with a step size of 1 μm. Data acquisition was conducted on cross-sections parallel to the RD-ND plane, i.e. the plane normal to the TD direction. The EBSD measurements were used to generate texture data using the Oxford HKL acquisition and analysis software. Characterization of inclusions was performed using backscattered electron imaging in a scanning electron microscopy (SEM) combined with energy dispersive spectroscopy (EDS). This was done using the INCA Steel software interface to automatically characterize the inclusions with regards to composition, quantity and size.

3. Results and Discussion

3.1 Influence of calcium treatment on macrostructure

A typical chemical composition of the liquid steel is given in **Table 2**. As explained earlier, one of the sheet samples was used to study the morphology of the inclusions using SEM. **Figure 1** shows a SEM image of the surface of a sheet sample from coil A in **Table 2**. **Figure 1 (a)** highlights the niobium carbide (NbC) and titanium nitride (TiN) inclusions. At a higher magnification (5000X), in **Figure 1 (b)**, an Al_2O_3 -MgO spinel inclusion enveloped by TiN is apparent. Figure 1(c) and Figure 1(d) shows the EDS spectra of the spinel inclusion core and TiN respectively. Various additions of calcium-containing wire were made resulting in calcium concentrations ranging from 0 to 2.1 times the standard content. The calcium contents and the application of EMS are given in **Table 3.** **Figure 2** shows that calcium content and EMS have a clear effect on the percentage of equiaxed grains in the slabs. As shown in **Figure 3** slab A, with no EMS but no calcium treatment, is almost 100 % equiaxed. However, this heat was difficult to cast due to clogging of the SEN: the SEN had to be replaced after casting one heat, whereas 4-5 heats are normally cast in sequence using the same SEN. Sample E with 2 times to the standard calcium content and without EMS is only 10% equiaxed. The EGR of the samples from slabs where EMS was applied (B, C and D) also decreased as their calcium content increased. When it was applied, the EMS power was constant for all the heats.

3.2 Calcium treatment and inclusion characterization

The compositions of all the inclusions were treated numerically to remove the contributions from nitrides and carbides. The remaining oxides of Al, Ca, and Mg contents were than assumed to correspond to Al_2O_3, MgO and CaO and normalized to 100% and plotted on a Al_2O_3-MgO-CaO ternary phase diagram as shown in **Figure 4 (a-e).** The isothermal section of the Al_2O_3-MgO-CaO

ternary diagram at 1873K (1600^{o} C) together with a projection of the liquidus temperatures is shown in **Figure 4f.** From the ternary diagram of sample A, it is clear that the inclusions are mainly of Al_2O_3-MgO spinel crystals and they were mostly solid prior to the solidification of the steel, and as mentioned in the earlier section, this heat was difficult to cast due to clogging of the SEN. These inclusions also provide favorable surfaces for the nucleation of titanium nitrides, which, in turn favorable for nucleating δ-ferrite grains thereby increasing the EGR. Inclusion compositions in sample B are shown in **(Figure 4b)**. This heat has been treated with a standard amount of calcium, which resulted in a shift in the inclusion composition from the spinel region to the liquid + spinel region of the phase diagram. With increased calcium treatment, inclusion compositions in samples (C to E), shifted more towards the liquid region, **Figure 4 (c-e)**, which further improved the casting conditions but also reduced the EGR as shown earlier.

3.3 Ridging

The surfaces of all the ridging test samples are shown in **Figure 5** showing the severity of ridging. The surface roughness profiles of the samples after ridging are shown in **Figure 6a and 6b**. The surface roughness parameters evaluated from the ridging profiles and their ridging indices (RI) are given in **Table 4**. The degree of ridging (RI) correlates with the Rz values but also takes the spacing between the ridges into account. RI for samples A and B is very small (0.7), moderate for samples C and D (1.9 and 2.4), and large in sample E (6.1). The RI values of the samples are inversely proportional to the percentage of equiaxed grains in the slab. However, ridging is not entirely eliminated with even 100% EGR in sample A and B. Nevertheless, the severity of ridging is negligible when the RI is less than 1. With only about 10% EGR, sample E has the highest susceptibility to ridging with the ridging index of 6.1 more than 8 times that of sample A and B. It is well known that materials with high susceptibility to ridging cannot be used in deep drawing applications due to the increased production costs that result from the additional mechanical

polishing needed to achieve a enough high quality surface finish on the products. In the present case, material from sample E would fail to meet requirements, while C and D would perform moderately.

3.4 Micro-texture analysis

Figure 7 shows the inverse pole figure maps of the TD-ND cross section of the entire thickness of the samples, which comprised recrystallized equiaxed grains. The grain sizes are different mainly in samples D and E where the calcium content has been high at 2 and 2.1 times to sample A, although EMS has been on during the casting of sample D and off for the sample E. The grain size distributions are shown in **Figure 8**. The mean grain sizes of specimens A-C are 11.5, 18.6 and 11.9 µm, while D and E have larger grain sizes at 46.3 and 38.5 µm, respectively. The grain size is directly correlated to the percentage of equiaxed grains in the slabs and the amount of cold reduction: the higher the slab EGR and the total cold reduction, the smaller the mean grain size. In samples D and E due to higher content of Ca during ladle furnace treatment the columnar grain zone is increased which are difficult to recrystallize leading to larger grain sizes.

In the IPF maps, the red denotes the grains with the orientation <100>//ND (cube-on-face) and the blue denotes <111>//ND oriented grains. As can be seen from the IPF maps, the frequency of grain in the cube-on-face orientation increases through the series A to E. The grains in the cube-on-face orientation are well dispersed over the entire thickness unlike in sample D where the cube oriented grains are near the surface and reducing towards the center. In sample-E with highest ridging, the cube oriented grains are spread all over the thickness and equal amount of alpha <011>//ND (α-fiber oriented grains are also representing a substantial percentage along the center line.

For quantitative analysis of the textures, orientation distribution functions (ODFs), i.e. f(g), were calculated from the EBSD data considering each orientation g = {φ_1, ϕ, φ_2} with a half scatter width of 5^o in Euler space. The resulting ODFs are presented in **Figure 9**. A and B have the strongest {111}//ND texture with f(g)max = 11 followed by C with f(g) = 8.3, D has f(g)=6.7 and E with f(g) =5.3. Specimen D also has a high α-fiber strength, higher than E. **Figure 10** shows the development of final texture along the α-fiber and γ-fiber of the specimens. The γ-fiber intensity is clearly highest in A and B, moderate in C and lowest in D and E while the opposite trend is true of the α-fiber intensity.

3.5 Effect of Ca treatment and EMS

The slabs of FSS without any titanium addition comprise mainly coarse columnar grains; a fine equiaxed solidification structure is only obtained when a suitable titanium addition is made.[28] In the actual steelmaking process, TiN, Al_2O_3-MgO spinel inclusions aggregate and cause nozzle clogging. To overcome this problem Ca treatment is applied to change the solid alumina inclusions into liquid calcium aluminate inclusions, but this treatment has an adverse effect on the fraction of equiaxed structure. The slab structure of A, as shown in **Figure 2**, is like that commonly shown in the literature for stabilized FSS without EMS and without Ca treatment: the solidification structure is mainly equiaxed.

The inclusions of specimen A **(Figure 4)** are mainly have an Al2O3-MgO spinel phase composition. The crystal lattice disregistry between spinel and TiN is very low[7], hence the spinel particles accelerate the formation of TiN in the steel melt. Bramfitt[30] studied the effect of various carbide and nitride additions on the nucleation of δ-ferrite in liquid iron and found that TiN and TiC were the most effective. This is attributed to the good lattice registry between these phases

and {100} planes of δ-ferrite, thereby promoting an equiaxed grain structure. Specimen B, which had the lowest calcium content of all the calcium treated heats also contained Al_2O_3-MgO spinel inclusions to promote the equiaxed grain structure; however, it also contained liquid CaO-Al_2O_3-MgO inclusions to reduce the clogging. When the Ca content is further increased by factors of 1.8, 2.1 and 2.0 with respect to specimen B, i.e. specimens C, D and E, the EGR steadily decreased. The inclusion characterization showed that the reason for this is the reduction in the incidence of the spinel inclusions in favor of the liquid CaO-Al_2O_3-MgO inclusions. Thus, TiN nucleation is delayed as the favorable spinel inclusions are not readily available and so the nucleation of δ-ferrite to promote an equiaxed grain structure is less efficient.

The nucleation of δ-ferrite on TiN increases equiaxed structure but decreases the cast-ability of the melt due to clogging at SEN. An alternative approach to promote grain refinement is mechanically by stirring the molten metal with sufficient force, where EMS is used. Melt stirring induces grain refinement by: (1) allowing the flow to penetrate the mushy zone partially re-melting the dendritic arm necks and the tips of dendritic crystals may break free from the leading edge of the mushy zone and be carried away by the melt stream. These grain fragments become the sites for new grains. (2) Thermal gradient in the liquid is lowered, thus extending the undercooled region and favoring a columnar to equiaxed transition.[31-33] In this study, along with Ca treatment, effect of EMS is also studied by applying EMS to the heats of specimens B, C and D, but not E. Considering the macro-textures of specimens B-E, B has almost the same EGR as A. The inclusions in B are a mixture of spinel (Al_2O_3-MgO) and liquid CaO-Al_2O_3-MgO, thus promoting equiaxed grain structure right after the chill layer of the casting, after which EMS has further promoted equiaxed grain nucleation and growth[6,32,33] On the other hand, comparing C and E, the lack of TiN leads to columnar grain growth after the chill layer in E, but not in C, where the equiaxed zone is promoted by the EMS. The unfavorable inclusion composition due to the high

calcium content and lack of EMS in E leads to the lowest EGR of all the specimens – the slab is entirely columnar. As can be seen from specimens B, C and D, even when EMS is applied, the percentage of equiaxed grains steadily decreases with increasing Ca content.

The fraction of columnar grains <100> // ND was highest and so the ridging severity is also highest in D and E compared to the other specimens. As is widely acknowledged, ridging is caused by the differences in the plastic deformation behavior of grains with different textures. It is well known that plastic strain ratio (r-value) depends on crystal orientation: the r-value for the α-fibre orientations {001} <100>, [001} <110> and {112} <110> orientations is relatively low compared to that of the ϒ-fiber {111} <uvw> orientations. [34–36] Therefore, local texture variations cause locally varying r-values, which results in the occurrence of ridging. Zhang et al[37]crystal plasticity finite-element simulation results conducted using EBSD data indicated that grains along α-fibre have lower r-values compared to the grain along γ-fibre. The same can be observed from the **Figure 10** that the sample D and E has very low intensity of {111} <uvw> and higher intensity of {hkl} // <110> orientations.

As shown in Table-1, A, B C and E are cold rolled twice with an intermediate annealing step while specimen D has been cold rolled only once. It is well known that intermediate annealing and high cold reduction ratios promote the {111}//ND (ϒ-fiber) texture,[36,38] which improves the formability and the resistance to ridging. On the contrary, in the case of slabs with low equiaxed grain ratios, intermediate annealing during cold rolling is unable to improve the resistance to ridging.

4. Conclusions

Production trials were conducted to study the effect of calcium treatment in the ladle furnace and electromagnetic stirring during casting on the slab solidification structure and the ridging resistance of titanium-niobium stabilized ferritic stainless steels. The effect of intermediate annealing during cold rolling on ridging was also been studied.

In the absence of calcium, even without EMS, cast slabs contain a high ratio of equiaxed grains and the final cold-rolled and annealed sheet shows little ridging. By using EMS, it is possible to add a small quantity of calcium to reduce the tendency to nozzle clogging and still achieve the same level of low or ridging free properties in the final product. However, a calcium concentration of 2 times the standard level already leads to lower fractions of equiaxed grains after casting and a greater tendency to ridging in the final product even if EMS is used.

Poor resistance to ridging can be attributed to the presence of a strong cube-on-face texture in the final sheet as a result of a low equiaxed grain ratio in the cast structure, whereas a strong ϒ-fiber and weak cube-on-face texture results in better resistance to ridging. In the case of slabs with low equiaxed grain ratio, intermediate annealing during cold rolling is unable to improve the resistance to ridging.

Acknowledgements

The authors gratefully acknowledge the support of Outokumpu Stainless Oy for the test materials and permission to publish the article.

References

[1] H.-C. Chao, *Trans. ASM*. **1967**, *60,* 37–50.

[2] R.N. Wright, *Metall. Trans.*, **1972**, *Vol. 3*, 83-91. https://doi.org/10.1007/BF02680588.

[3] Y. Itoh, T. Okajima, H. Maede, K. Tashiro, *Trans. Iron Steel Inst. Japan*. **1982**, *22*, 223–229. https://doi.org/10.2355/isijinternational1966.22.223.

[4] H. Shibata, S. Itoyama, Y. Kishimoto, S. Takeuchi, H. Sekiguchi, *ISIJ Int*. **2006,** *46,* 921–930. https://doi.org/10.2355/isijinternational.46.921.

[5] J. Hutt, D. Stjohn, *Int. J Cast Metal*. **1998**, *11,* 13–22. https://doi.org/10.1080/13640461.1998.11819254.

[6] J.C. Kim, J.J. Kim, J.Y. Choi, J.H. Choi, S.K. Kim, *Metall. Ital.* **2009**, *101,* 43–48.

[7] H. Fujimura, S. Tsuge, Y. Komizo, T. Nishizawa, *Tetsu-To-Hagane,* **2001**, *87*, 29–34. https://doi.org/10.2355/tetsutohagane1955.87.11_707.

[8] T. Koseki, H. Inoue, *J. Jpn. Inst. Met.,* **2001**, 644–651.

[9] H.P. Wang, L.F. Sun, J.J. Shi, C.J. Liu, M.F. Jiang, C. Zhang, *Rare Met*. **2014,** *33,* 761–766. https://doi.org/10.1007/s12598-013-0150-x.

[10] S.-B. Lee, J.-H. Choi, H.-G. Lee, P.C.-H. Rhee, S.-M. Jung, *Metall. Mater. Trans B*. **2005,** *36,* 414–416. https://doi.org/10.1007/s11663-005-0071-7.

[11] M.A. Van Ende, M. Guo, J. Proost, B. Blanpain, P. Wollants, *ISIJ Int.* **2011***, 51,* 27–34. https://doi.org/10.2355/isijinternational.51.27.

[12] J.J. Pak, J.O. Jo, S.I. Kim, W.Y. Kim, T.I. Chung, S.M. Seo, J.H. Park, D.S. Kim *ISIJ Int*. **2007**, *47,* 16–24. https://doi.org/10.2355/isijinternational.47.16.

[13] B.G. Thomas, H. Bai, Steelmaking. Conf. Proc., ISS, Warrendale, PA, **2001.**

[14] K.G. Rackers, B.G. Thomas, Proc. 78th Steelmaking Conf., Nashville, TN, **1995**, 723-734.

[15] S. Basu, S.K. Choudhary, N.U. Girase, *ISIJ Intl*., **2004**, *44,* 1653–1660. https://doi.org/10.2355/isijinternational.44.1653.

[16] C.W. Seo, S.H. Kim, S.K. Jo, M.O. Suk, S.M. Byun, *Metall. Mater. Trans B,* **2010**, *41,* 790–797. https://doi.org/10.1007/s11663-010-9377-1.

[17] D.C. Park, I.H. Jung, P.C.H. Rhee, H.G. Lee, *ISIJ Int*., **2004**, *44,* 1669–1678. https://doi.org/10.2355/isijinternational.44.1669.

[18] H. Itoh, M. Hino, S. Ban-Ya, *Metall. Mater. Trans B,* **1997**, 28, 953–956. https://doi.org/10.1007/s11663-997-0023-5.

[19] H. Ohta, H. Suito, *Metall. Mater. Trans B,* **1997**, 28, 1131–1139. https://doi.org/10.1007/s11663-997-0069-4.

[20] L. Holappa, M. Hämäläinen, M. Liukkonen, M. Lind, *Ironmak. Steelmak*., **2003,** *30*, 111-115. https://doi.org/10.1179/030192303225001748.

[21] G. Ye, P. Jönsson, T. Lund, *ISIJ Int*. **1996**, *36.* https://doi.org/10.2355/isijinternational.36.suppl_s105.

[22] J. Hyun Park, D. Sik Kim, S. Lee, *ISIJ Int*. 2000, 47, 16-24. https://doi.org/10.2355/isijinternational.47.16.

[23] W. Yang, L. Zhang, X. Wang, Y. Ren, X. Liu, Q. Shan, *ISIJ Int*. **2013**, *53,* 1401–1410. https://doi.org/10.2355/isijinternational.53.1401.

[24] M. Jiang, X. Wang, B. Chen, W. Wang, *ISIJ Int*., **2010***, 50,* 95–104. https://doi.org/10.2355/isijinternational.50.95.

[25] P.B.P. Leão, J.L. Klug, C.A.R. Carneiro, H. Caldas, W. v. Bielefeldt, *Steel Res. Int.* **2019**, 90, 1–10. https://doi.org/10.1002/srin.201900151.

[26] J. Li, G. Cheng, Q. Ruan, J. Pan, X. Chen, *Metall. Mater. Trans B,*. **2018**, 49B, 2357-2369. https://doi.org/10.1007/s11663-018-1331-7.

[27] J. Li, G. Cheng, Q. Ruan, J. Pan, X. Chen, *Metall. Mater. Trans B.* **2018***, 49*, 2018-2357. https://doi.org/10.1080/03019233.2019.1568367.

[28] X. Shi, L. Chang, *High Temp.* **2018**, *37*, 951–959. https://doi.org/10.1515/htmp-2017-0173.

[29] S. Kodukula, T. Ohligschläger, D. Porter, *ISIJ Int., **2021**,* 61, 1–7. https://doi.org/10.2355/isijinternational.ISIJINT-2020-137.

[30] B.L. Bramfitt, Metall. Trans. **1970, 1** 1987–1995. https://doi.org/10.1007/BF02642799.

[31] J.D. Hunt, Steady state columnar and equiaxed growth of dendrites and eutectic, *Mater. Sci. Eng.,* **1984**, 65, 75–83. https://doi.org/https://doi.org/10.1016/0025-5416(84)90201-5.

[32] T. Campanella, C. Charbon, M. Rappaz, *Metall. Mater. Trans A.*, **2004,** 35 A, 3201–3210. https://doi.org/10.1007/s11661-004-0064-1.

[33] C.J. Paradies, R.N. Smith, M.E. Glicksman, *Metall. Mater. Trans A.*, **1997**, 28, 875–883. https://doi.org/10.1007/s11661-997-1016-3.

[34] R.K. Ray, J.J. Jonas, R.E. Hook, *Int. Mater. Rev.*, **1994**, 39 129–172. https://doi.org/10.1179/imr.1994.39.4.129.

[35] D.N. Lee, K.H. Oh, *J Mater Sci*., **1985, 20** 3111–3118. https://doi.org/10.1007/BF00545175.

[36] I. Jung, J. Mola, D. Chae, B.C. de Cooman, *Steel Res Int*., **2010, 81,** 1089–1096. https://doi.org/10.1002/srin.201000125.

[37] C. Zhang, Y. Xu, L. Zhang, X. Zhou, *Steel Res Int*., (2020), 2000109, 1–12. https://doi.org/10.1002/srin.202000109.

[38] M.-Y. Huh, O. Engler, Mater Sci Eng A., **2001**, 308, 74–87. https://doi.org/10.1016/S0921-5093(00)01995-X.

Figures

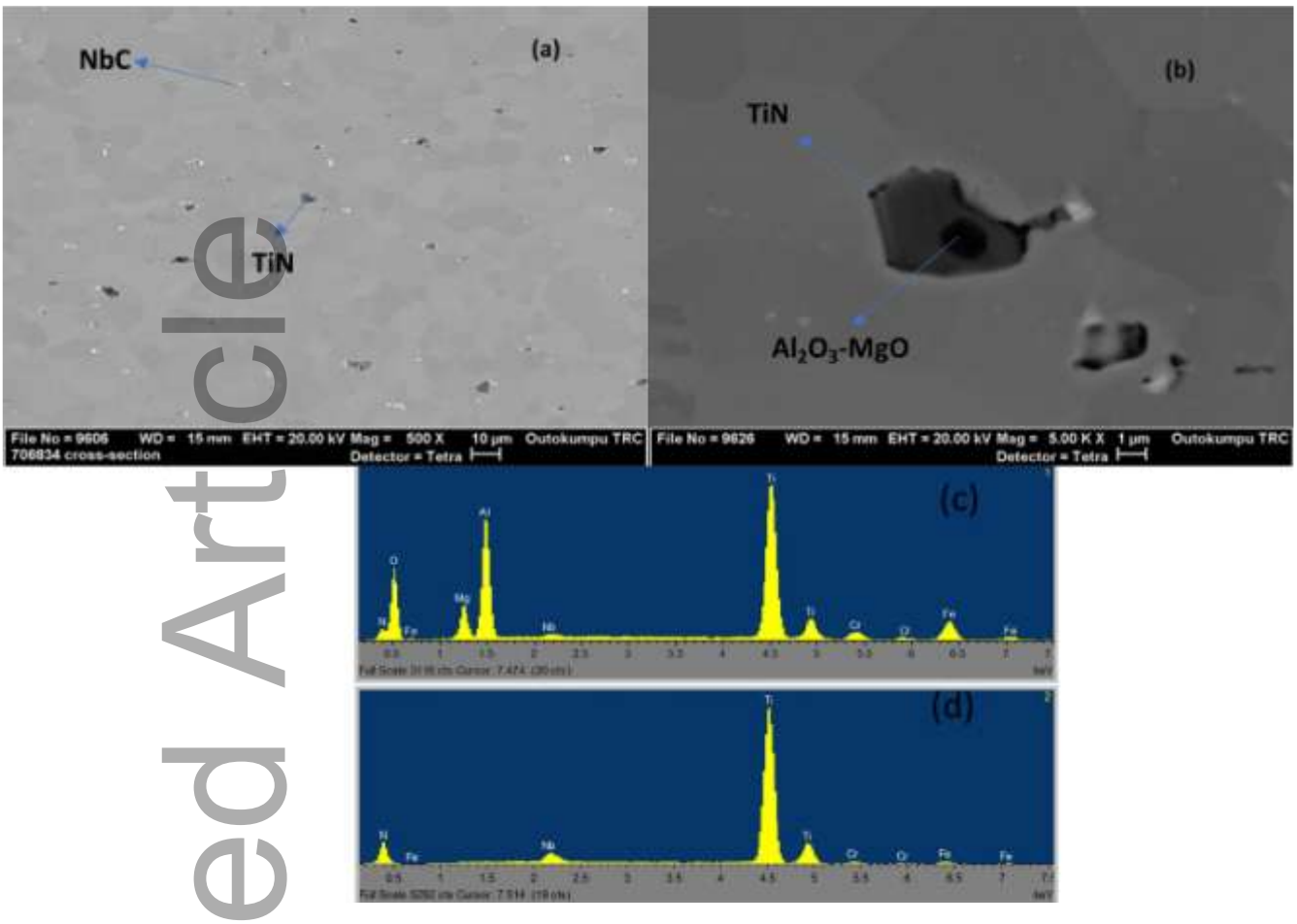

Figure 1 a) SEM image of a sheet specimen from coil A showing TiN and NbC inclusions. b) TiN inclusion surrounding an Al_2O_3-MgO spinel inclusion. (c) EDS spectrum of the core of the TiN inclusion revealing the spinel composition (d) TiN inclusion

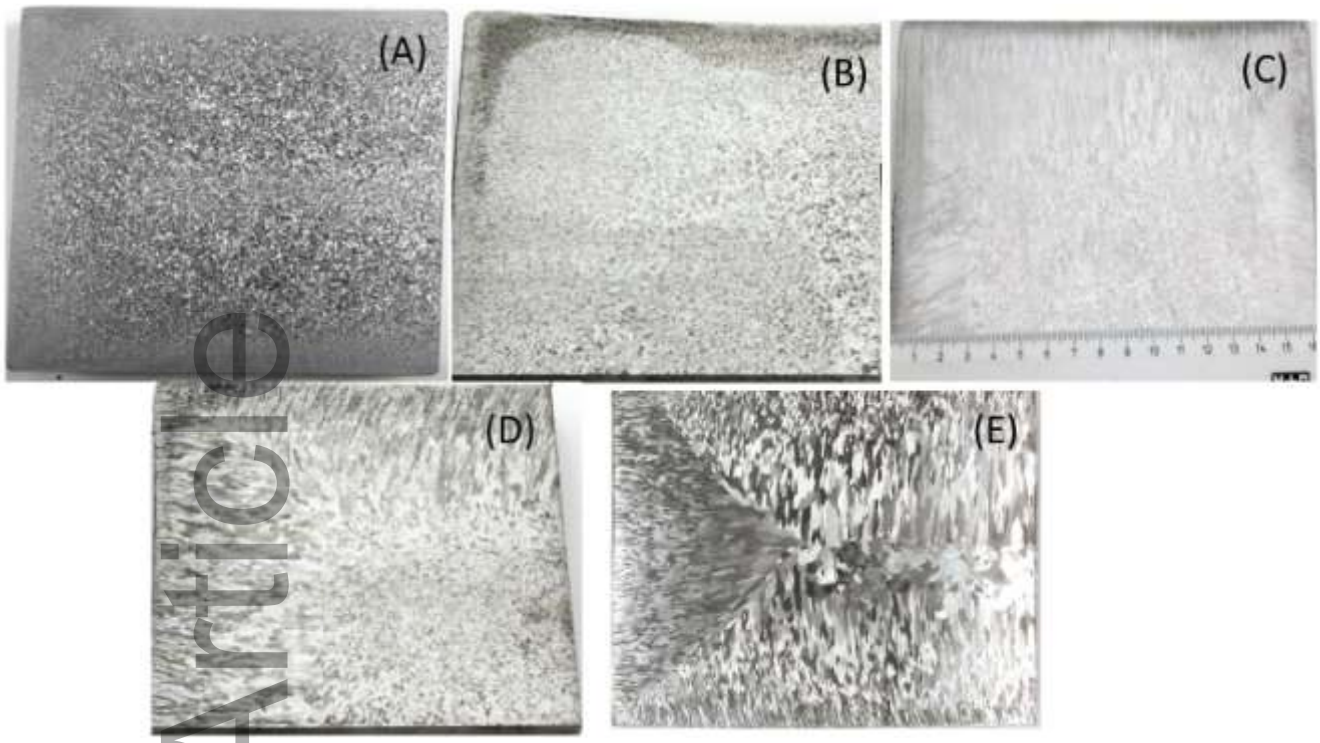

Figure 2. Slab cross-section images after macro-etching

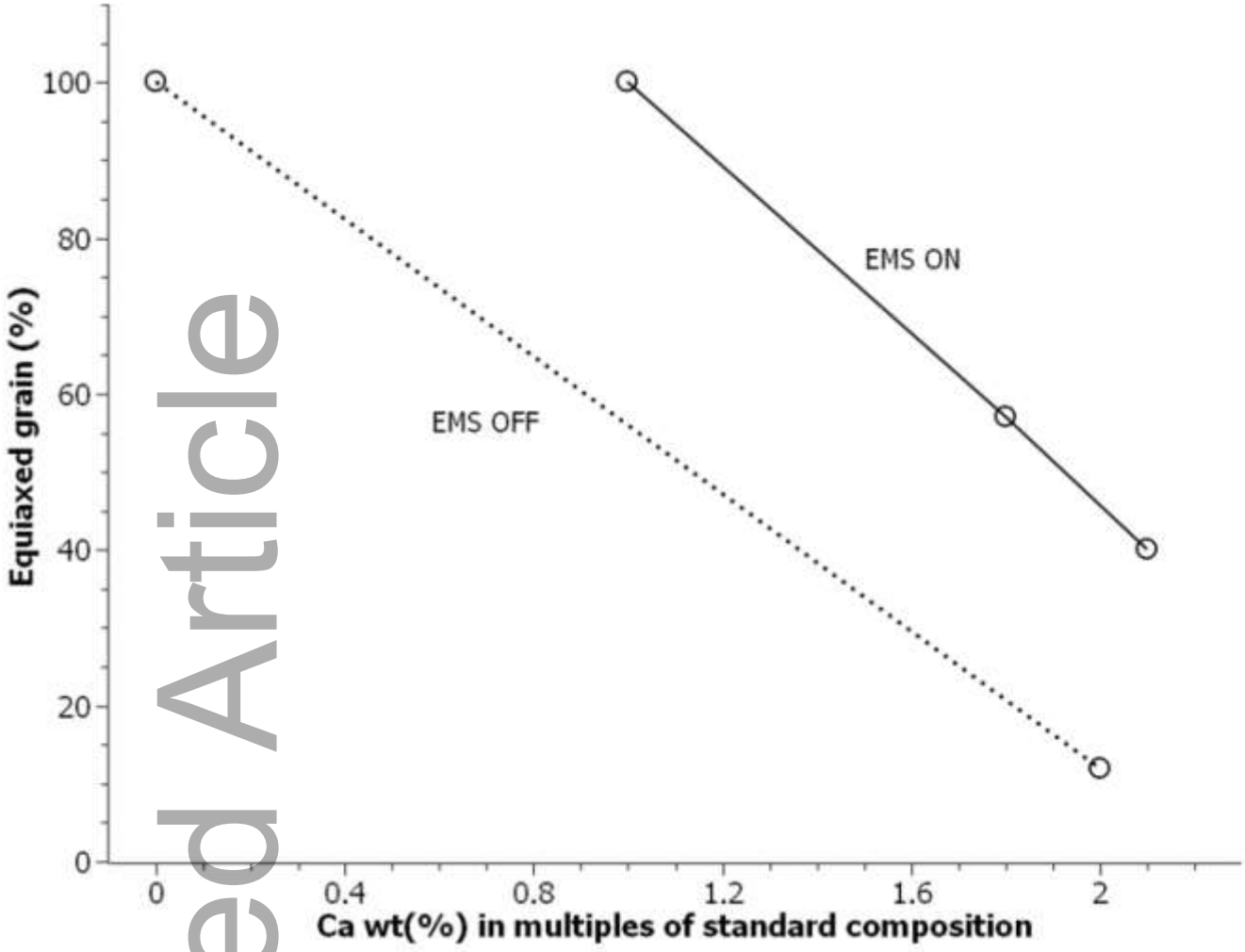

Figure 3. Effect of calcium content and EMS on slab equiaxed grain ratio (EGR).

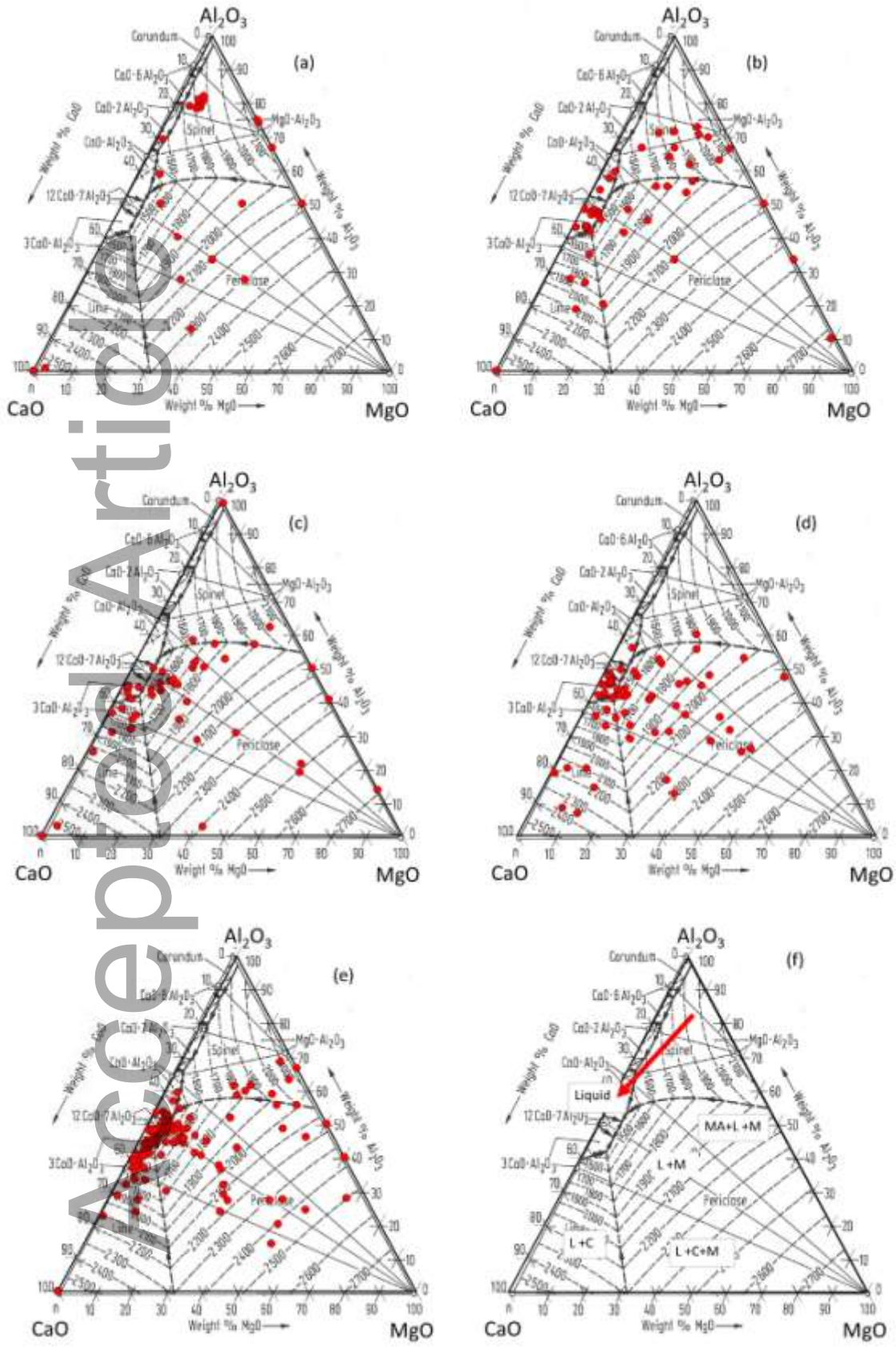

Figure 4 (a-e) Compositions of inclusions from specimens A-E plotted on a ternary diagram showing a combination of 1873 K (1600^{o} C) isotherm of the Al2O3-MgO-CaO ternary phase diagram and projected liquidus temperatures. (f) Isothermal section of the Al2O3-MgO-CaO

ternary diagram at 1873 K (1600^{o} C). Arrow indicates the desired inclusion composition after the calcium treatment. (A=Al_2O_3, Mg=MgO, C= CaO and L = liquid)

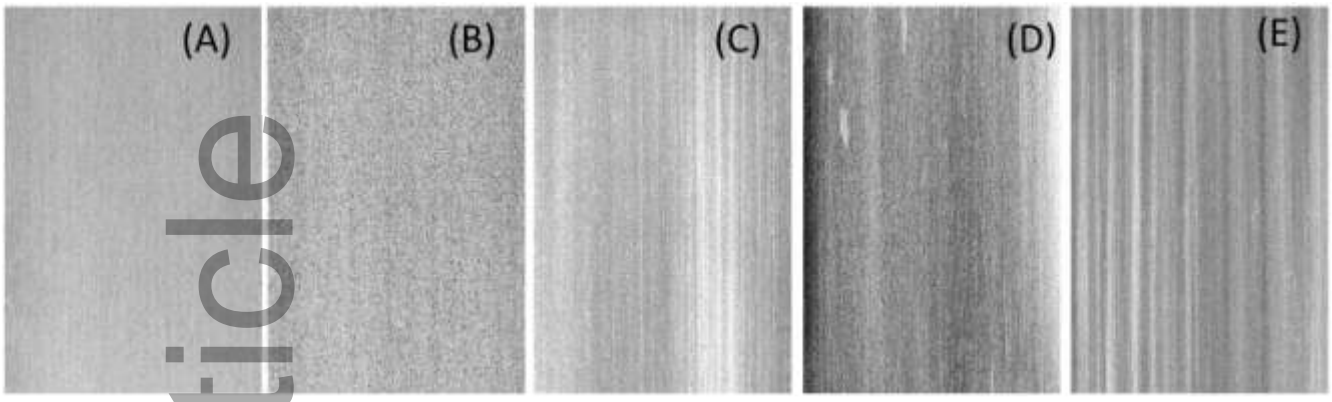

Figure 5. The surfaces of the ridging test specimens after 15 % elongation in the rolling direction.

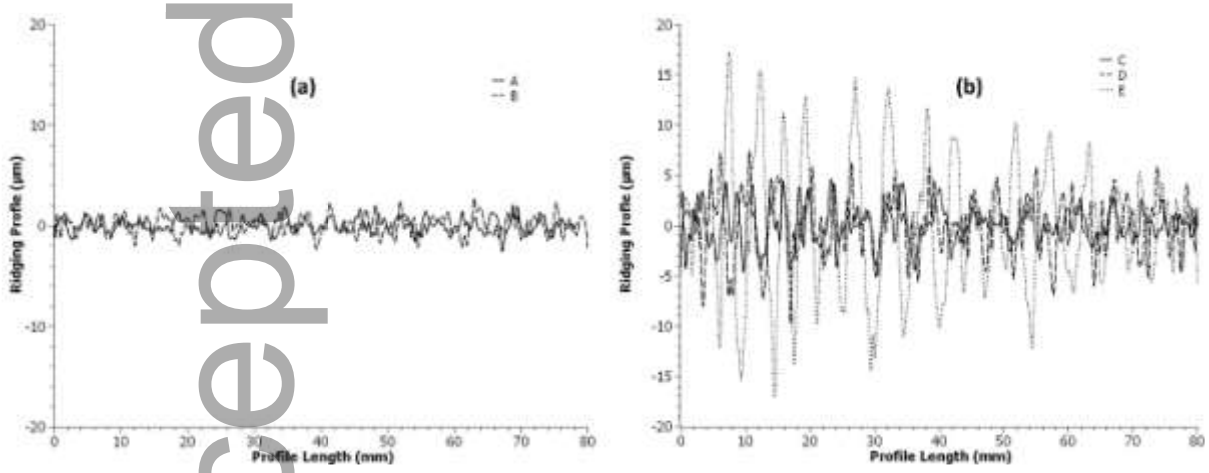

Figure 6. Ridging profiles (a) Specimen A has (EMS-off and no calcium) and B has (EMS-on) and the standard amount of Ca (b) Specimens C, D have EMS on E have EMS off. C, D and E have calcium contents of 1.8, 2.1, and 2.0 times the standard Ca level.

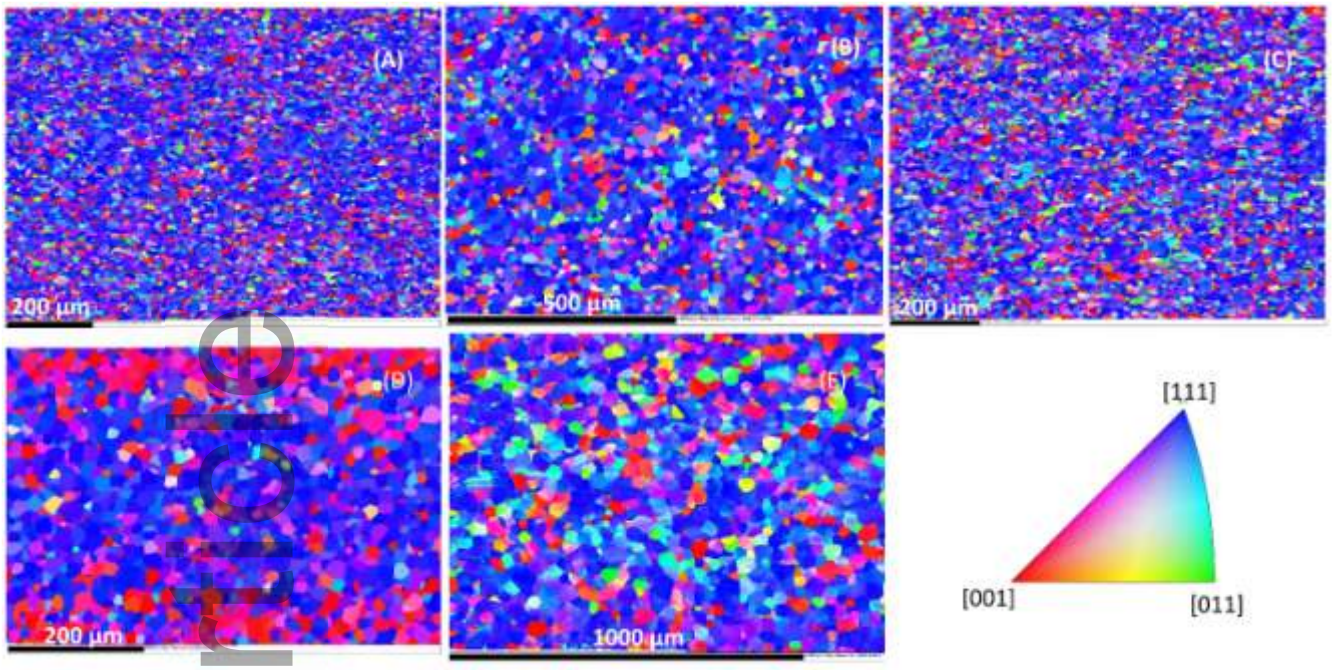

Figure 7. EBSD-IPF images of TD-ND cross-sections of the final cold-rolled and annealed sheets. Colors represent the orientation of the ND.

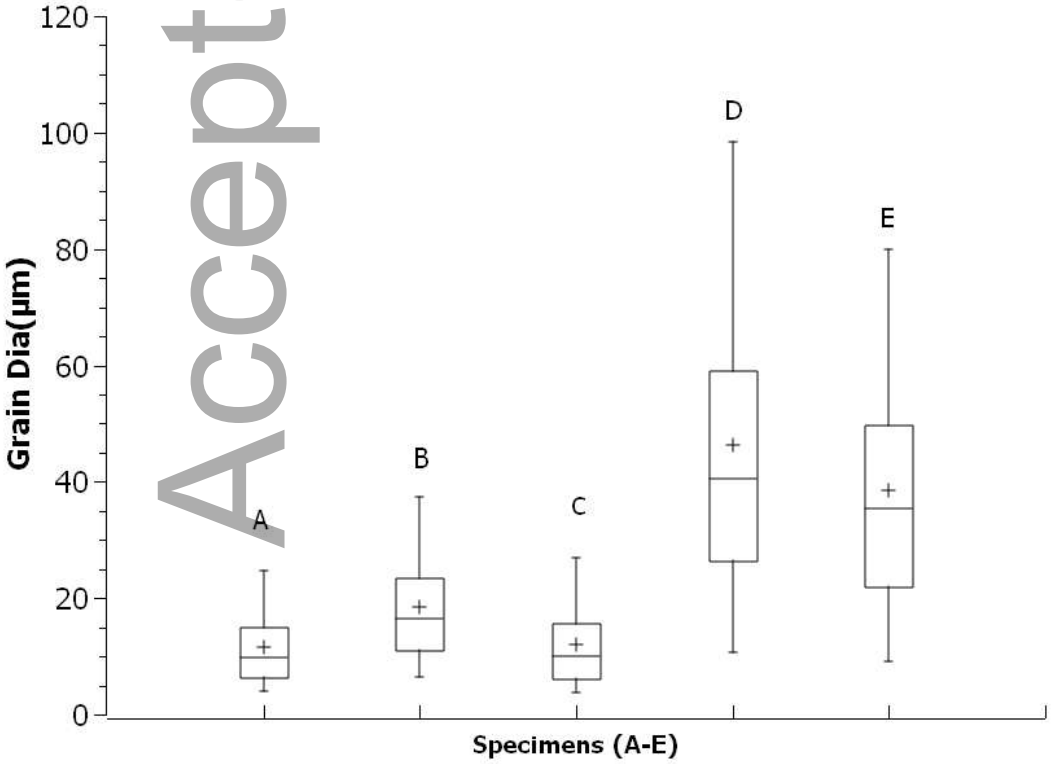

Figure 8. Grain size distributions. The rectangle indicates 25th, 50th and 75th percentile and the whiskers indicate the 5th and 95th percentile of the grain size distributions. (+) indicates the mean grain sizes

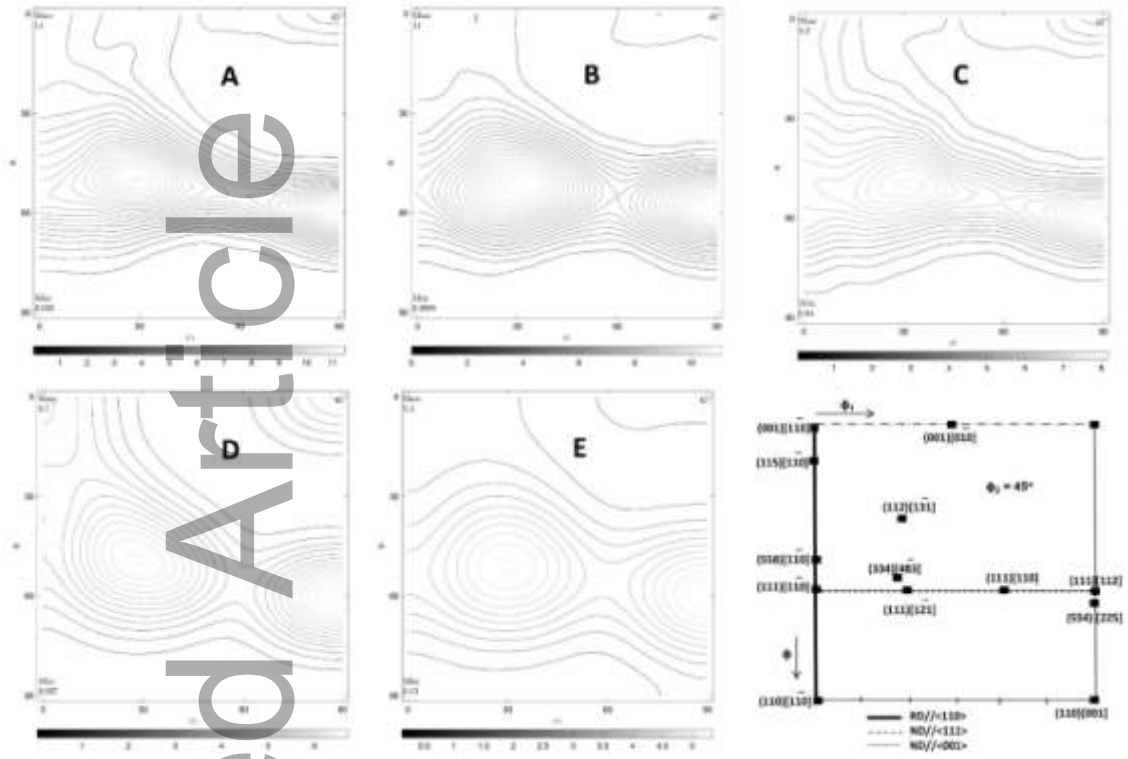

Figure 9. ODF sections of samples A-E at Φ_2=45^{o}. Each contour represents a step of 0.5

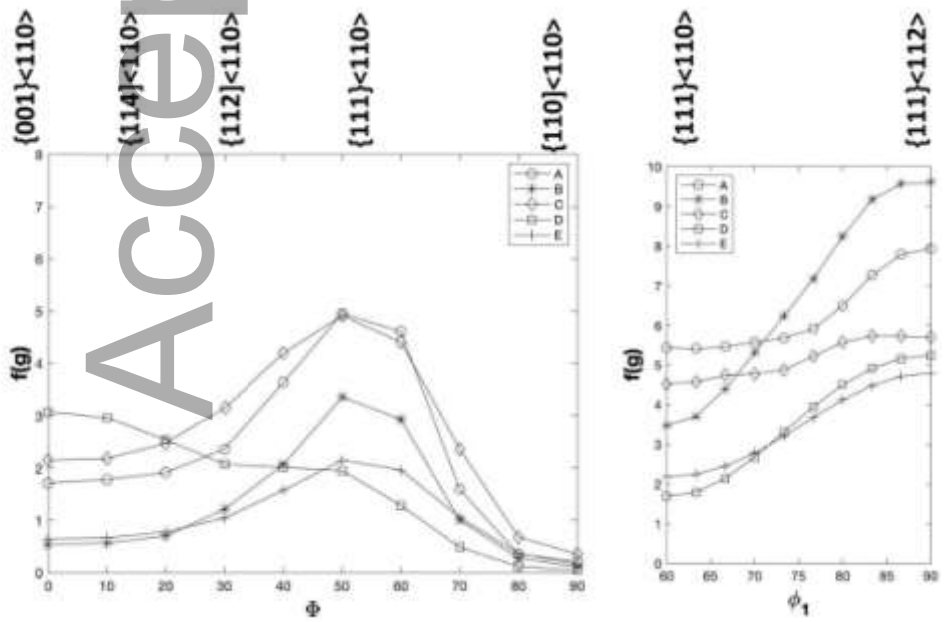

Figure 10 a) α-fiber intensities b) γ-fiber intensities

Tables

Table 1 Hot and cold rolling thicknesses and reductions.

Sample	HR thickness (mm)	Final thickness (mm)	Total cold reduction (%)
A	6.0	0.70	88
B	6.0	0.70	88
C	6.0	0.68	89
D	3.5	1.17	67
E	6.0	1.02	83

Table 2. Typical chemical compositions of the slabs in weight %.

C	N	Cr	Si	Mn	Ti	Nb
0.022	0.025	17.6	0.37	0.50	0.10	0.40

Table 3. EMS parameters and Ca content in multiples of the standard content.

Sample	EMS	Ca treatment	Ca (ppm)
A	Off	No	-
B	On	Yes	1.0
C	On	Yes	1.8
D	On	Yes	2.1
E	Off	Yes	2.0

Table 4 Surface roughness parameters calculated from the ridging profiles.

Sample	Ra (µm)	Rz (µm)	RI
A	0.42	3.30	0.7
B	0.63	4.30	0.7
C	0.60	7.60	1.9
D	1.41	13.5	2.4
E	1.23	24.4	6.1

Keywords: Calcium Treatment, Ridging, Electromagnetic Stirring, Titanium and Niobium Stabilization

Suresh Kodukula*, Marko Petäjäjärvi, Jari Savolainen, Timo Fabritius, David Porter

Title: Influence of calcium treatment and electromagnetic stirring on ridging of dual-stabilized Ferritic Stainless Steels

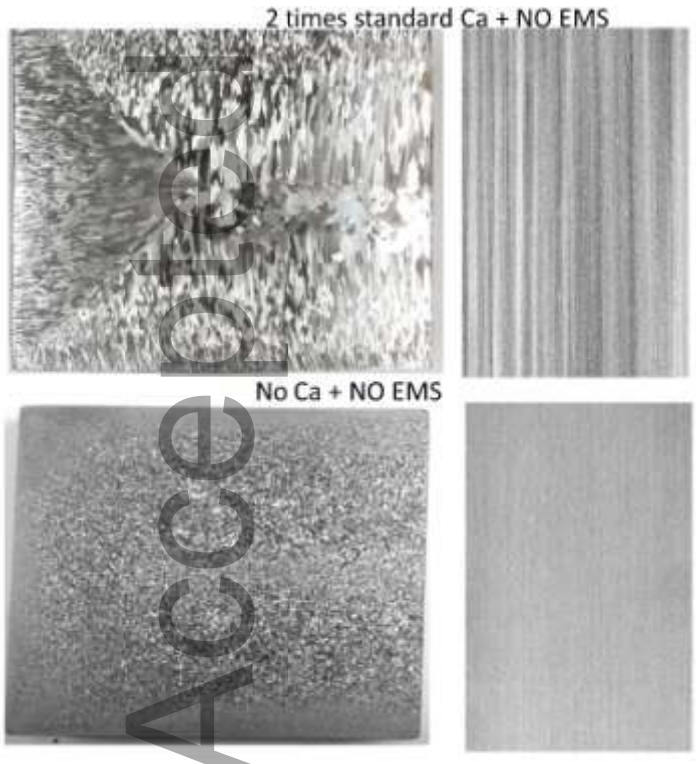

Short summary:

The effect of calcium treatment and electromagnetic stirring is investigated in dual stabilized (Ti and Nb) ferritic stainless steels. The combined effect of the amount of calcium added during ladle

furnace treatment and EMS during continuous casting on equiaxed grain ratio of the cast structures was studied. The final product performance towards the ridging resistance has been investigated with reference to the cast structure.